

Well-Organized Zeolite Nanocrystal Aggregates with Interconnected Hierarchically Micro–Meso–Macropore Systems Showing Enhanced Catalytic Performance

Xiao-Yu Yang,^{*,[a, b, e]} Ge Tian,^[b] Li-Hua Chen,^[b] Yu Li,^[a, b] Joanna C. Rooke,^[b] Ying-Xu Wei,^[c] Zhong-Min Liu,^{*,[c]} Zhao Deng,^[a] Gustaaf Van Tendeloo,^[d] and Bao-Lian Su^{*,[a, b]}

Abstract: Preparation and characterization of well-organized zeolitic nanocrystal aggregates with an interconnected hierarchically micro–meso–macroporous system are described. Amorphous nanoparticles in bimodal aluminosilicates were directly transformed into highly crystalline nanosized zeolites, as well as acting as scaffold template. All pores on three length scales incorporated in one solid body are interconnected with each other. These zeolitic nanocrystal aggregates with hi-

erarchically micro–meso–macroporous structure were thoroughly characterized. TEM images and ²⁹Si NMR spectra showed that the amorphous phase of the initial material had been completely replaced by nanocrystals to give a micro–meso–macroporous crystalline

Keywords: crystal growth • heterogeneous catalysis • mesoporous materials • microporous materials • zeolites

zeolitic structure. Catalytic testing demonstrated their superiority due to the highly active sites and the presence of interconnected micro–meso–macroporosity in the cracking of bulky 1,3,5-triisopropylbenzene (TIPB) compared to traditional zeolite catalysts. This synthesis strategy was extended to prepare various zeolitic nanocrystal aggregates (ZSM-5, Beta, TS-1, etc.) with well-organized hierarchical micro–meso–macroporous structures.

Introduction

Zeolites have excellent thermal, hydrothermal, and chemical stability and have been successfully employed in vapor-phase chemistry.^[1] However their use is much less frequent in organic reactions, as the size of the molecules can exceed the size of the small zeolite pores.^[1–3] Thus, zeolite materials

with controlled shape and porosity are preferred to minimize diffusion limitations. Recently, various successful attempts to synthesize mesoporous or macroporous zeolites with bimodal porosity and framework acidity have been reported.^[4–15] These materials hold great promise, particularly in catalysis and separation processes in which optimization of the diffusion and confinement regimes is required. Whereas micro- and/or mesopores provide size and shape selectivity for the guest molecules, and thus enhance the host–guest interactions, the presence of macropores can considerably favor diffusion of the guest molecules and thus their access to the active sites.^[1,16–36] This is particularly important for the diffusion of large molecules or in viscous systems. However, these conventional as-synthesized zeolite catalysts are usually extruded with inorganic binders to make them suitable for practical applications. Several attempts have already been made in this field;^[37,38] for example, 3D macroporous monolithic silicalite-1 by using polymer spheres,^[39] and hierarchically structured monolithic zeolites by using a carbon template.^[40–42] In these cases, the organic scaffold templates must be removed by calcination. It would therefore be interesting to develop a more facile and organic scaffold free route to self-supporting well-organized zeolite nanocrystal aggregates with interconnected hierarchically micro–meso–macroporous systems. Ideally, such materials should have both well-defined macropores and interconnected mesopores within walls which have been constructed from tunable microporous units. More importantly,

[a] Dr. X.-Y. Yang, Dr. Y. Li, Dr. Z. Deng, Prof. Dr. B.-L. Su
State Key Laboratory of Advanced Technology for
Material Synthesis and Processing
Wuhan University of Technology
Luoshi Road 122, Wuhan 430070 (P.R. China)

[b] Dr. X.-Y. Yang, Dr. G. Tian, Dr. L.-H. Chen, Dr. Y. Li,
Dr. J. C. Rooke, Prof. Dr. B.-L. Su
Laboratory of Inorganic Materials Chemistry (CMI)
University of Namur (FUNDP), 61, rue de Bruxelles,
5000 Namur (Belgium)
Fax: (+32)81-725414
E-mail: xyyang@fundp.ac.be
liuzm@dicp.ac.cn
bao-lian.su@fundp.ac.be

[c] Dr. Y.-X. Wei, Prof. Dr. Z.-M. Liu
Dalian National Laboratory for Clean Energy
Dalian Institute of Chemical Physics, Chinese Academy of Sciences

[d] Prof. Dr. G. Van Tendeloo
EMAT, University of Antwerp, Groenenborgerlaan 171
B-2020 Antwerpen (Belgium)

[e] Dr. X.-Y. Yang
Chargé de recherche
FNRS (Fonds National de la Recherche Scientifique)

on all length scales, the larger pores should be connected to the smaller pores, to result in a greater range of potential applications, such as the fluidized catalytic cracking process. Here we describe the synthesis and characterization of zeolite nanocrystal aggregates with interconnected hierarchically micro–meso–macroporous systems prepared by a quasi-solid-state crystallization process. These hierarchically porous materials are constructed from zeolite nanocrystals and exhibit high catalytic activity. The general synthesis procedure is illustrated in Figure 1. A meso–macroporous aluminosilicate,^[36] which could be easily synthesized without any external template, was mixed with a structure-directing agent, such as tetrapropylammonium (TPA⁺), to aid zeolite formation. A supplementary silica source was added to facilitate transformation of the amorphous phase of the meso–macroporous aluminosilicate into a crystalline micro–meso–macroporous aluminosilicate with zeolite ZSM-5 architecture. The initial meso–macroporous aluminosilicate acted as

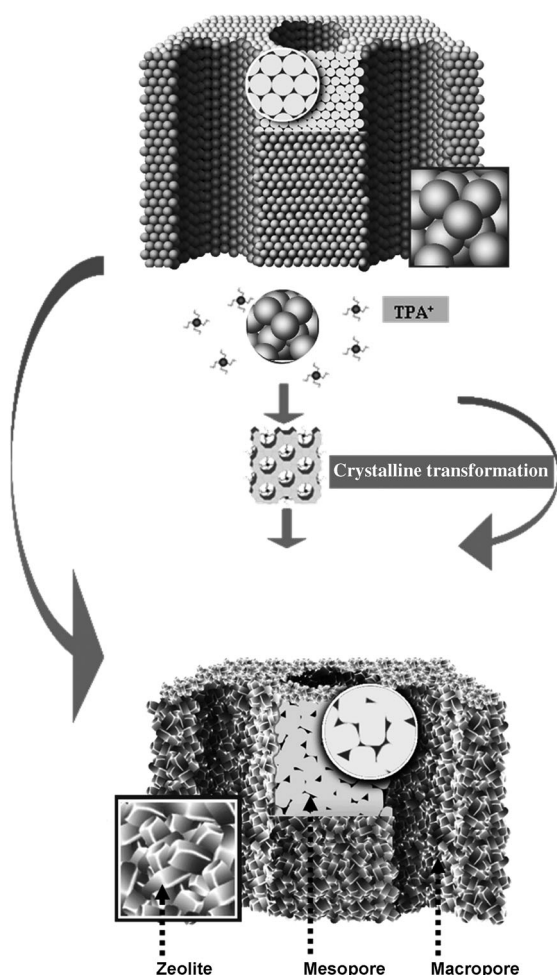


Figure 1. Schematic representation of the synthesis of hierarchically micro–meso–macroporous aluminosilicates constructed from zeolite nanocrystals by a quasi-solid-state crystallization process. Top: The initial meso–macroporous aluminosilicates constructed from amorphous particles (inset). Middle: The quasi-solid-state crystallization process from an amorphous framework to a crystalline framework by means of a structure-directing agent (TPA⁺) and glycerol. Bottom: Micro–meso–macroporous aluminosilicates constructed from zeolite nanocrystals (inset).

silica and alumina source, as well as scaffold template. During the transformation, the macroporosity was not affected and thus entirely transferred to the final materials constructed from nanocrystals. The resultant material has pores on three length scales: a well-defined macroporous structure with highly interconnected mesopores, which developed during the growth of the microporous zeolite nanocrystals on the basis of the mesoporosity of the precursor materials, and micropores which could be tailored by controlling the zeolite type. Most importantly, the resultant materials not only have stable catalytically active sites due to the microporous zeolites, but also bulky molecules can easily diffuse into the macropores and access the channels of the mesopores and make contact with these active sites. These multimodal porous materials constructed from zeolite nanocrystals are highly desired in the design of hierarchically porous zeolites. The key to the design was to find a suitable crystallization process that not only transformed the amorphous phase into zeolite crystals but also protected the meso–macroporous structure. The structure of the meso–macroporous aluminosilicate would be easily destroyed during conventional hydrothermal reactions owing to its amorphous framework. The question then arises whether an atypical hydrothermal process can be used for the synthesis, that is, a method that minimizes the damage to the mesoporous and macroporous structure caused by hydrothermal synthesis. Some successful methods were demonstrated by Kanno et al., Campos et al., Coppens et al., and Kaliaguine et al.,^[24,25,43–50] who used glycerol as a medium to directly synthesize zeolites, to recrystallize mesoporous silica to zeolite, to embed zeolite nanocrystals into a well-connected amorphous matrix, and to coat the walls of mesostructured materials with zeolite nanoclusters, respectively. However, the generation of crystalline micro–meso–macroporous aluminosilicates constructed entirely from zeolite nanocrystals with interconnectivity on three length scales still remains a great challenge, since the structures of the mesoporous aluminosilicates would still be easily destroyed during reactions even when using the glycerol system. In spite of the lack of entirely crystalline nanosized zeolites with direct interconnectivity of meso- or macroporosity, reflected by TEM images, this is still an interesting idea, as it can provide a new and mild synthesis route to introduce zeolite structures into mesostructured bodies, and thus minimize the damage caused by hydrothermal synthesis owing the recrystallization process of the multiporous structure. The crystallization process was performed under quasi-solid-state conditions by using mixture of dried gel and glycerol, as opposed to fully hydrothermal conditions with water. As the glycerol becomes more fluidlike it acts as a flux which improves Brownian motion, aiding the diffusion of solid particles, a rate-determining step in solid-state chemistry. This meant that the structure-directing agent could still strongly interact with growing crystal domains, through the formation of covalent bonds with other SiO₂ and Al₂O₃ sources, yet by fine-tuning the synthetic system, that is, the synthetic gel, medium, temperature, and so on, the mesoporous and macroporous struc-

tures could be preserved. This method uses glycerol as it would not attack the amorphous aluminosilicate network to the same degree that H₂O would at high vapor pressures, yet as it is heated it becomes less viscous and thus plays the role of water. The quasi-solid-state crystallization process in glycerol system was thus employed to transform the nano-sized amorphous particles into crystalline zeolites, and thereby govern the mesoporosity within the meso-macroporous aluminosilicate to yield an unprecedented well-organized zeolite nanocrystal aggregate with interconnected hierarchically micro-meso-macroporous system. Another advantage of this chemical crystallization process is that it enables aggregation or condensation of zeolite nanocrystals with each other, which is a critical factor to avoid collapse of the walls of the macropores. Moreover, the smaller mesopores of the initial meso-macro-porous aluminosilicates appear to be governed by nanoparticle aggregation, which is in contrast to the mesoporous materials used by the above-mentioned groups. While the amorphous walls and original mesopores gradually disappeared with increasing reaction time, larger mesopores were generated. The microporous zeolite crystals possibly grew by using the amorphous phase as a source to create a new mesostructure. The key to this synthesis is that the macroporous structure can easily be maintained during the transformation, owing to relatively thick walls (ca. 2–5 μm).

Results and Discussion

Studies by SEM and TEM (Figures 2 and 3) revealed that a well-organized hierarchically micro-meso-macroporous architecture was formed at 130 °C through post-crystallization synthesis over various reaction periods (initial, 1 d, and 2 d,

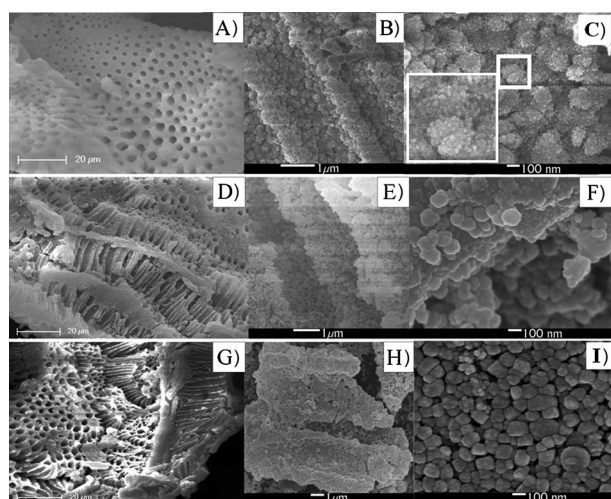


Figure 2. SEM investigation of the formation of micro-meso-macroporous aluminosilicate. A–C) MMM(0), D–F) MMM(1), G–I) MMM(2), corresponding proposed schematic drawing (Figure 1) of initial precursor (C) and final product (I) and high-magnification image of the same particles (inset of C). Scale bars: A, D, G) 20 μm , B, E, H) 1 μm , C, F, I) 100 nm.

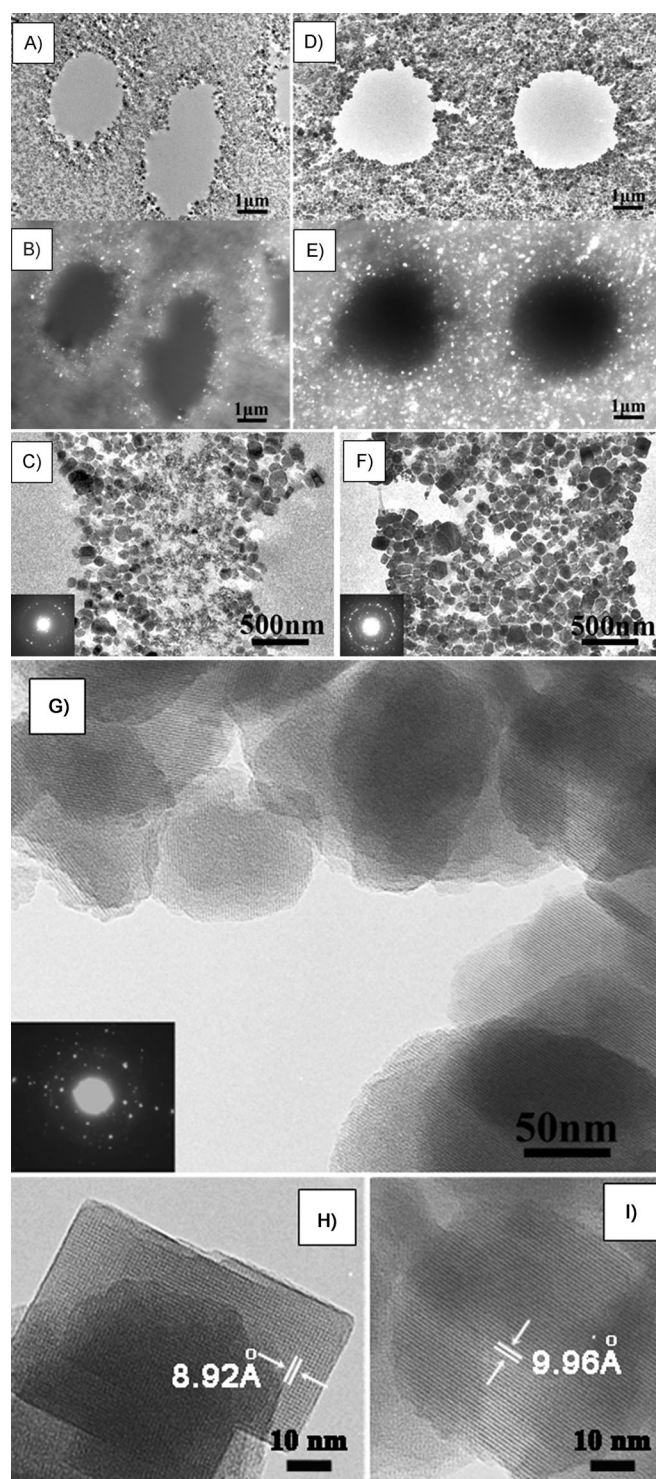


Figure 3. TEM investigation of the formation of micro-meso-macroporous aluminosilicate. A–C) correspond to MMM(1) with A) bright-field and B) dark-field images taken on the same area and C) a higher-magnification view of A). D–F) correspond to MMM(2) with D) bright-field and E) dark-field images taken on the same area and F) a higher-magnification image of D). G–I) HRTEM images of MMM(2). The insets in C), F), and G) are the corresponding selected-area electron diffraction patterns taken from numerous particles. Scale bars: A, B, D, E) 1 μm , C, F) 500 nm, G) 50 nm, H, I) 10 nm.

designated MMM(0), MMM(1), and MMM(2), respectively). The precursor material exhibits a macroscopic network with relatively homogenous and straight channel-shaped macropores of 2–5 μm in diameter. The macrochannels are arranged parallel to each other (Figure 2A and B). The walls around the macrochannels are composed of very homogenous particles of about 150 nm in size (Figure 2B and C and inset), which result in interparticle porosity. These particles are themselves formed by aggregation of smaller nanoparticles (Figure 2C and inset) and thus have accessible smaller mesovoids, similar to previously reported meso-macroporous materials.^[36] As the reaction time proceeded (1 d), material MMM(1) retained its meso-macroporous structure (Figure 2D–F) and zeolite MFI nanoparticles began to form on the macropore walls (Figure 2F, Figure 3A). The dark-field TEM image (Figure 3B) was acquired on the same region as the bright-field TEM image (Figure 3A). The bright spots in the image correspond to MFI nanocrystals (Figure 3B). Figure 3C shows the wall separating two macrochannels. The crystalline zone and the remaining amorphous phase are easily distinguishable. The nanocrystals that developed around the macropore walls gradually embedded themselves within the continuous amorphous inorganic matrix and thus formed a new crystalline framework while preserving the meso- and macroporous scaffold (Figure 3A–C). These zeolite MFI particles, located within the framework of the meso-macroporous aluminosilicate precursor (Figure 2G–I, Figure 3D) became more crystalline after 2 d at 130 °C. Notably, the bright-field image (Figure 3D) showed that the amorphous phase of the initial material had been completely replaced by the nanocrystals and thus suggests that this process aided the crystallization of the amorphous framework leading to a micro-meso-macroporous aluminosilicate structure. Crystallization or the transformation of amorphous aluminosilicate phase into well-crystallized zeolite phase did not affect the meso-macroporous framework of the precursor (Figure 2G and H). The parallel macrochannel structure is well preserved. The dark-field image (Figure 3E) further indicated that the meso-macroporous framework was mainly crystalline, owing to the presence of bright spots corresponding to the MFI nanocrystals fully occupying the matrix. Figure 3F shows an image of the wall separating two macrochannels, which is clearly composed of an assembly of nanocrystals. In addition, higher-magnification TEM images (Figure 3F and G) and circular streaking in the electron diffraction pattern (inset of Figure 3G) indicated that the micro-meso-macroporous aluminosilicates were constructed from randomly oriented zeolite nanocrystals. Furthermore, high-resolution (HR) TEM studies (Figure 3G–I, H and I) confirm that the sample has very uniform nanocrystals with high crystallinity observed by SEM (Figure 2G). The ZSM-5 nanoparticles in the macroporous wall of MMM(3) show a high degree of crystallinity, and the lattice fringes of 0.892 (Figure 3H) and 0.996 nm (Figure 3I) correspond to the (210) and (200) crystal planes of the tetragonal structure of ZSM-5 (JCPDS card no. 044-0002), respectively. Electron microscopy investiga-

tion revealed that the amorphous domain gradually disappeared with increasing reaction time, and subsequently larger mesopores and voids, compared to the initial mesopores, were generated. Owing to the effect of the structure-directing agent TPA^+ , the microporous zeolite crystals were able to grow by using the amorphous phase as a source of aluminum and silicon atoms to create new mesostructure. Interestingly, the entirely zeolite architecture exhibits a uniform zeolite crystal size of about 150 nm (Figure 2I and Figure 3D, F–I), and this results in relatively uniform mesopores or mesovoids, which lead to improved catalytic activity. The crystal size of 150 nm is approximately the same size as that of the amorphous aggregate of nanoparticles found in the precursor material (ca. 150–200 nm, see Figure 2C). Moreover, TEM studies (Figure 3C and F) reveal that the nanocrystals of the surface of the macroporous channels did not grow excessively with increasing reaction time, while the crystal size remained around 150 nm. This phenomenon is unique, and quite different from other routes reported previously.^[24–25, 43–50] As the size of the microporous zeolite crystal formed is similar to that of the starting amorphous aggregate of nanoparticles, this could potentially indicate that each aggregate of nanoparticles was transformed into a zeolite crystal, possibly due to good accessibility for the structure-directing agent and supplementary silica source of the unique mesostructure formed by aggregation of the nanoparticle precursor and the relatively mild glycerol system. This is probably a critical factor in the formation of uniform crystals and maintenance of the mesostructure. The macroporous structure was also unaffected due to the relatively thick macroporous wall in the meso-macroporous aluminosilicate and relatively mild reaction system (Figures 2G–I and 3B–F). This indicates that the overall meso-macroporous structure within the initial material was maintained during the transformation (Figures 2 and 3). Furthermore, even after calcination at 550 °C for 5 h, the nanocrystals in macroporous walls do not obviously aggregate with each other, and thus the mesopores or mesovoids are not affected (Figure 3). This means that the hierarchical materials have highly thermal stability, which is mostly important for recycling. In summary these observations clearly suggest that a hierarchically micro-meso-macroporous material which has well-defined macropores and interconnecting mesopores within the macropore walls was constructed from zeolite nanocrystals with tunable micropores.

Figure 4 shows XRD patterns of micro-meso-macroporous aluminosilicates MMM(0), MMM(1), and MMM(2) synthesized at 130 °C. Notably, the peaks in the XRD patterns of samples MMM(1) and MMM(2) are characteristic of ZSM-5 crystal symmetry (JCPDS card no. 044-0002), and the enhanced wide-angle XRD pattern suggested that the degree of crystallinity gradually increased and the amorphous phase of the precursor gradually disappeared with increasing reaction time (Figure 4). These results are in good agreement with the electron microscopy investigation.

Figure 5 shows N_2 adsorption isotherms of MMM(0), MMM(1), and MMM(2) calcined at 550 °C. The isotherm

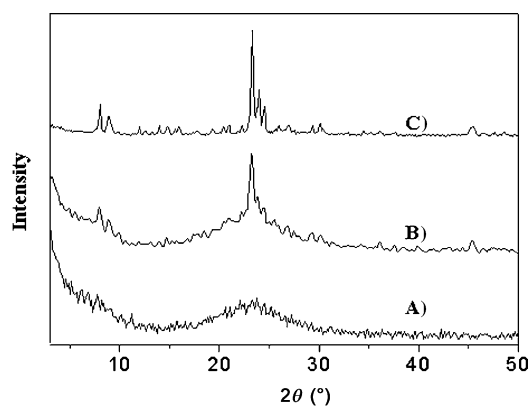


Figure 4. Wide-angle XRD patterns of A) MMM(0), B) MMM(1), and C) MMM(2).

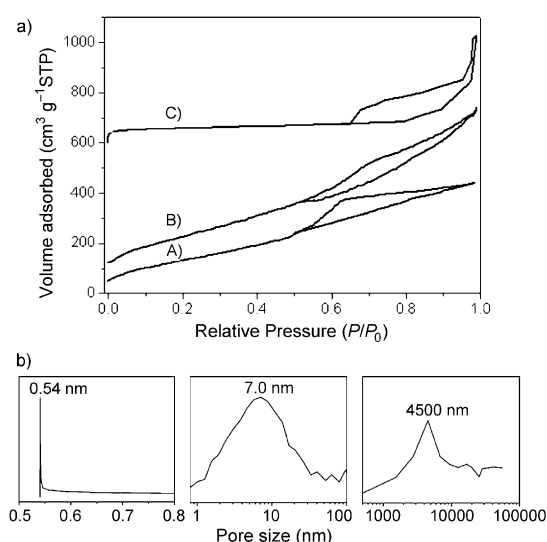


Figure 5. Top: N_2 isotherms of calcined samples. A) MMM(0), B) MMM(1), and C) MMM(2). Isotherms B and C are offset by $100 \text{ cm}^3 \text{ g}^{-1}$ and $600 \text{ cm}^3 \text{ g}^{-1}$, respectively, along the vertical axis for clarity. Bottom: Pore size distributions of MMM(2) (macropore size distribution curve obtained by mercury porosimetry, and the micropore and mesopore size distribution curves obtained by nitrogen adsorption-desorption isotherms).

changed progressively from type IV to type I with increasing reaction time, and this suggests that the microporosity of the material gradually increased. The final material MMM(2) exhibits a type I isotherm with hysteresis at higher P/P_0 indicating clearly the presence of interparticle mesoporosity (Figure 5). The changes in isotherm shape and form, as well as the observation of hysteresis suggesting generation of microporosity, are in good agreement with TEM and XRD results. This was further confirmed by a ^{27}Al MAS NMR investigation (Figure 6). The sharp, symmetrical signal centered at about $\delta = 53 \text{ ppm}$, which corresponds to tetrahedral aluminum, was gradually enhanced with increasing reaction time. Simultaneously, the signal centered at about $\delta = 0 \text{ ppm}$, corresponding to an octahedral environment, was

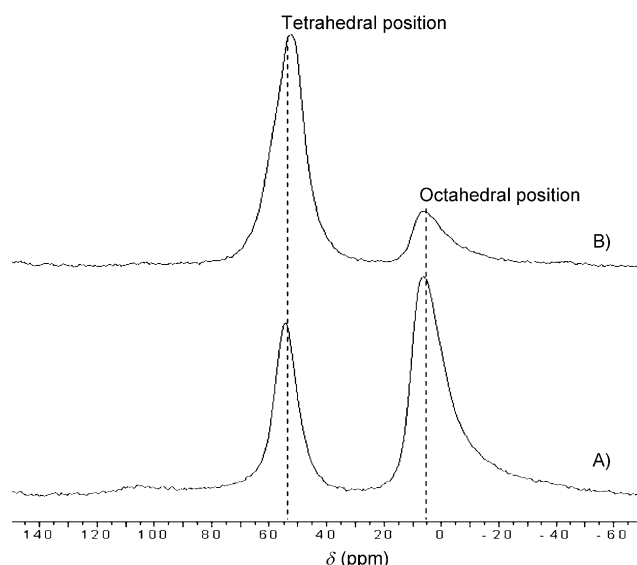


Figure 6. ^{27}Al MAS NMR spectra of A) calcined MMM(0) and B) calcined MMM(2).

correspondingly reduced. This indicates that the amorphous aluminum atoms were gradually incorporated into the micro-meso-macroporous framework in tetrahedral positions during the post-crystallization process. The transformation of Al atoms located in octahedral positions can be reasonably attributed to complete condensation of the amorphous domain during the zeolite crystallization process, which is further evidenced by ^{29}Si MAS NMR spectroscopy (Figure 7). Notably, the spectrum of the final material shows a highly intense resonance at $\delta = -112 \text{ ppm}$ and a shoulder peak at $\delta = -102 \text{ ppm}$ indicating that the micro-meso-macroporous material consists primarily of cross-linked Q^4 silica units [$\delta = -112 \text{ ppm}$, $\text{Si}(\text{OSi})_4$] and Q^3 units [$\delta = -102 \text{ ppm}$, $\text{Si}(\text{OSi})_3(\text{OH})$ and/or $\text{Si}(\text{OSi})_3(\text{OAl})$] as deduced from a very high Q^4/Q^3 ratio of 5. No Q^2 units were observed. In contrast, the initial material has typical peaks corresponding to Q^2 , Q^3 , and Q^4 silica species, with a $Q^4/(Q^3+Q^2)$ ratio of 1, revealing the presence of large amounts of amorphous aluminosilicate in the meso-macroporous framework. Complete condensation of the framework would result in more aluminum atoms on octahedral sites becoming tetrahedrally coordinated. This complete condensation may be attributed to the post-crystallization process, which could efficiently crystallize amorphous aluminosilicate to a crystalline zeolite phase.

The acidity of the samples (initial, 1 d, 2 d) was characterized by temperature-programmed desorption of ammonia (Figure 8). For comparison, commercial zeolite ZSM-5 and MMM(0) with similar Si/Al ratio (75–85) were also studied. All three samples show a large desorption peak at 150°C , corresponding to desorption of physisorbed NH_3 . Another desorption peak of ammonia, albeit small but evident on MMM(2), was located at about 560°C , and indicates strong acid sites on the product, similar to commercial zeolite ZSM-5 ($T_d = 520^\circ\text{C}$). In contrast, MMM(0) with a similar Si/

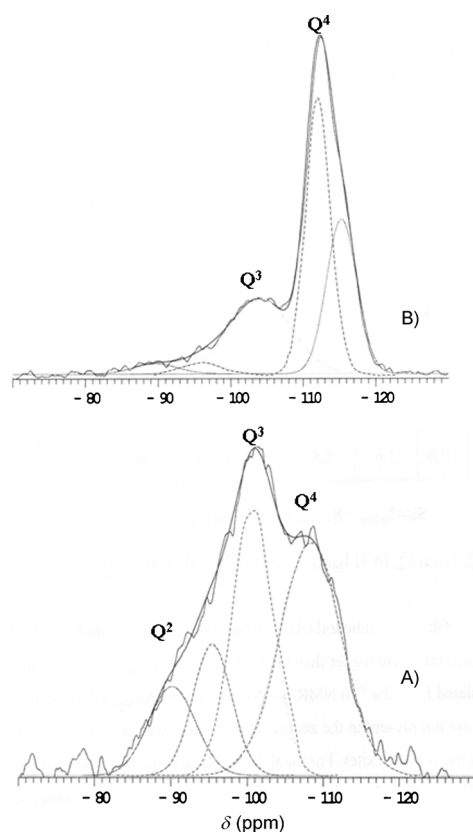


Figure 7. ^{29}Si MAS NMR spectra of A) calcined MMM(0) and B) calcined MMM(2).

Al ratio to MMM(2) and amorphous framework displayed a desorption peak at 450 °C, indicating weak acid sites. These results indicate that micro–meso–macroporous material MMM(2) has strong acidity, even stronger than that of commercial ZSM-5 crystals with similar Si/Al ratio, owing to full crystallization of the framework.

A micro–meso–macroporous structure with strong acidity has great advantages in catalytic reactions involving large organic molecules, as diffusion constraints and/or adsorption of reactant molecules onto the strong acid sites are the main concern. Catalytic activities for the cracking of the large-molecule hydrocarbon 1,3,5-triisopropylbenzene (TIPB) over various catalysts are compared and summarized in Table 1. The kinetic molecular dimension of TIPB is much larger than the entrance dimensions of MFI zeolites, and such molecules cannot penetrate into the internal channels of zeolite ZSM-5. Cracking reactions can thus be realized only at the external surface of ZSM-5 crystals. With a contact time of 24 ms, HZSM-5, a commercial product with Si/Al ratio around 75, is much less active (23.1%) owing to its relatively small pore size with respect to the large diameter of the reactant molecules. Al-MCM-41 and MCM-41 show no activity. In contrast, calcined MMM(2) with the same contact time yields the highest activity (88.6%). These observations further confirm that MMM(2) has strong acidity and high catalytic activity due to its greater porosity. Owing

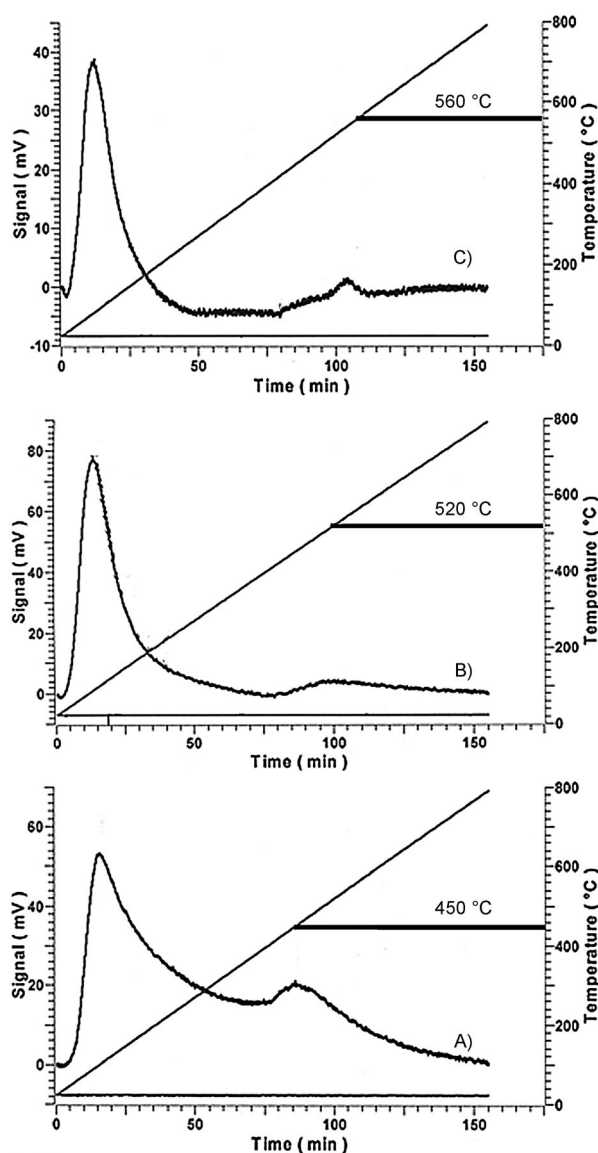


Figure 8. Temperature-programmed curves for the desorption of ammonia for A) MMM(0), B) ZSM-5, and C) MMM(2).

to the large size of the TIPB molecule, the cracking reaction on ZSM-5 zeolite crystals is independent of the contact time. The increase in contact time augments the diffusion effect in reaction systems. The advantages of micro–meso–macroporous zeolite architectures for reactions involving large organic molecules are evidenced. The presence of large meso–macroporosity favors the access of TIPB molecules to the active sites. The sharp increase in cracking activity clearly illustrates the superiority of MMM(2) as catalyst in TIPB cracking due to the increased diffusion effect. From Table 1, it is clear that the increase in contact time favors deep cracking of the TIPB reactant, as well as the IPB and DIPB intermediates formed during the reaction, to form propylene and benzene. No secondary reaction products are formed, since the cracking reaction was realized only at the external surface of the ZSM-5 catalyst. The MMM(2) cata-

Table 1. Catalytic activity for cracking of 1,3,5-triisopropylbenzene and the structural parameters obtained through BET measurements for various samples.^[a]

	Conv. [%]	Contact time [ms]	BET surface area [m ² g ⁻¹]	Si/Al	Product distribution [%]					
					P1	P2	P3	P4	P5	P6
MMM(2)	28.59	12	562	80	25.29	3.30	7.59	63.8	–	–
	44.46	18			25.91	3.01	6.57	62.86	–	1.64
	88.63	24			37.14	13.39	4.73	4.44	12.42	27.87
ZSM-5	17.25	12	302	75	40.75	16.98	25.51	16.75	–	–
	23.26	18			49.22	25.92	18.57	6.32	–	–
	23.97	24			24.48	26.41	16.85	5.59	–	–
Al-MCM-41	–	24	996	82	–	–	–	–	–	–
MCM-41	–	24	1075	∞	–	–	–	–	–	–

[a] Catalytic reactions were performed by pulse injection, and the data presented in this table are average values of five injections. Conditions for each run: catalyst (50 mg), pulse-injected reactant (0.4 μ L), flow rate 53.7 mL min⁻¹, temperature 350 °C. The products are propylene (P1), benzene (P2), isopropylbenzene (P3), diisopropylbenzene (P4), C₄–C₆ hydrocarbons (P5), and C₇–C₁₀ aromatics (P6). Samples were calcined at 550 °C for 5 h.

lyst not only facilitates the production of propylene and benzene, with increasing yield on increasing contact time, but also formation of secondary products such as C₄–C₆ hydrocarbons and C₇–C₁₀ aromatics, which stem from the cyclization and oligomerization of propylene during secondary reaction, can be observed in the mesopores and/or internal channels of ZSM-5 zeolite. This experiment clearly illustrates the benefits of hierarchically micro-meso-macroporous zeolite architectures, as in certain reaction systems a cascade of reactions can be carried out simultaneously by using different functionalities of catalyst. MMM(2) is thus an excellent candidate for a catalyst in industrial cracking of petroleum, particularly for petroleum residues, for which high reaction temperatures, large pore sizes, and cascade-type reactions are required to obtain products with high added value. Furthermore, this hierarchically micro-meso-macroporous aluminosilicate with zeolitic architecture, constructed from zeolite nanocrystals, may have important technological implications for many other catalytic reactions involving large molecules, whereas purely mesoporous or macroporous materials with amorphous frameworks lack the required acidity.

Synthesis of micro-meso-macroporous materials with zeolitic architecture by the post-crystallization process in glycerol system is not only limited to ZSM-5 zeolite. It could be successfully extended to the synthesis of micro-meso-macroporous zeolite beta (MMM(Beta), Figure 9A–D) and zeolite TS-1 (MMM(TS-1), Figure 9E and F)^[51, 52]. SEM and XRD studies reveal that zeolite beta and zeolite TS-1 architectures with meso-macroporous structure are successfully synthesized in the glycerol system (Figure 9), similar to the case of hierarchically micro-meso-macroporous aluminosilicate with zeolite ZSM-5 architecture. MMM(Beta) shows a type I isotherm (Figure 9C) with hysteresis at higher P/P_0 due to the presence of microporosity and interparticle mesoporosity. The ²⁷Al MAS NMR spectrum of MMM(Beta) (Figure 9D) shows a very strong peak around δ = 55 ppm, corresponding to tetrahedral Al sites in crystalline zeolite. It is believed that the strategy developed here provides a unique, effective, low-cost, and potentially

general approach for the synthesis of hierarchically micro-meso-macroporous materials with zeolitic architecture.

Conclusion

The current micro-meso-macroporous materials are the first examples of hierarchically micro-meso-macroporous aluminosilicates and titanosilicates with zeolitic architecture and strong acidity or interesting oxidation sites, obtained through a

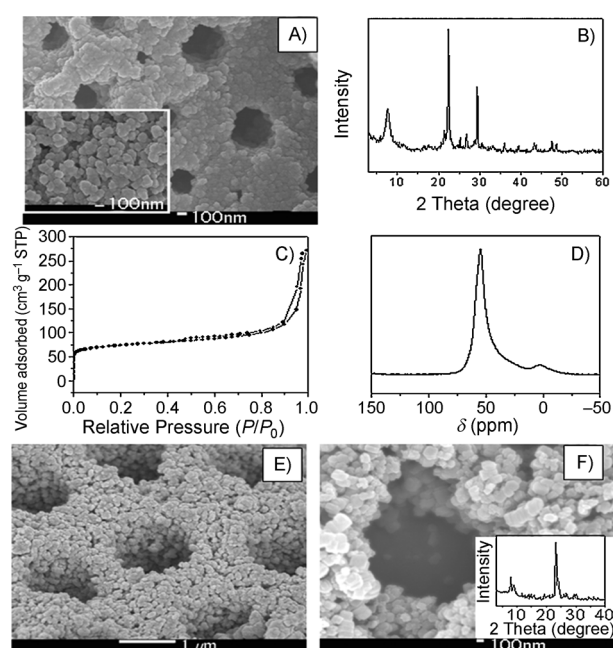


Figure 9. A) SEM image (inset: high magnification image), B) wide-angle XRD pattern, C) N₂ isotherm, and D) ²⁷Al MAS NMR spectrum of MMM(Beta). E, F) SEM images and wide-angle XRD patterns (inset of F) of MMM(TS-1). Scale bars: A) 100 nm, inset: 100 nm, E) 1 μ m, F) 100 nm.

post-crystallization process. They represent two significant advances in the search for new catalysts and candidates for catalyst supports. Firstly, these materials show a well-defined macroporous structure, which has a highly interconnected mesoporous system, in addition to the mesopores that developed during the growth of the microporous zeolite nanocrystals. Secondly, and more importantly, the zeolite type and its micropore size can be altered by a simple and clean method that could yield new insight into how the synthesis of these hierarchically micro-meso-macroporous materials can be controlled. Catalytic testing demonstrates their superiority in the cracking of 1,3,5-triisopropylbenzene (TIPB)

compared to traditional zeolite catalysts. This synthesis strategy is quite versatile, since hierarchically micro-meso-macroporous zeolite with beta and TS-1 architectures can be easily obtained.

Experimental Section

Typical synthesis: Step 1: An amorphous meso-macroporous aluminosilicate (designated MMM(0)) was synthesized from aluminum tri-*sec*-butoxide (TBOA, 12 g) and tetramethyl orthosilicate (TMOS, 30 g) in twice-distilled water.^[50] The solid product was dried directly at 50 °C for use as the precursor in step 2. Step 2: The dried precursor (1 g) was impregnated with 5.7 g TPAOH (40%), 15 g H₂O, 10 g TEOS, and 0.11 g NaAlO₂ and stirred for 4 h. After stirring and aging at RT, the gel was dried under vacuum at 70 °C. Finally, glycerol (5 g) was added and the gel was transferred to a Teflon-lined autoclave and heated at 130 °C for different periods of time (1 d: MMM(1), 2 d: MMM(2)). The products were washed with distilled water, dried in air at 60 °C, and finally calcined at 550 °C for 4 h to remove the organic residues. For the synthesis of TS-1 and beta zeolites, amorphous meso-macroporous aluminosilicate and titania-silica were used as starting materials. The zeolite beta sample (designated MMM(Beta)) was synthesized in the glycerol system after mixing and drying the amorphous meso-macroporous aluminosilicate and precursor with a molar ratio of Al₂O₃/SiO₂/TEAOH/H₂O of 1.0:60:25:800^[51], and micro-meso-macroporous TS-1 (designated MMM(TS-1)) was synthesized in the glycerol system after mixing and drying the amorphous meso-macroporous titania silica and precursor with a molar ratio TiO₂/SiO₂/TPAOH/C₂H₅OH/H₂O of 1.0:30:8:120:375.^[52]

X-ray diffraction patterns were obtained by using a Panalytical X'Pert diffractometer by using Cu_{Kα} radiation ($\lambda = 1.54056 \text{ \AA}$). Scanning electron microscopy was performed on a JSM-7500F electron microscope (JEOL, Japan). Transmission electron microscopy was performed by using a Philips CM20 with an acceleration voltage of 200 kV. High-resolution transmission electron microscopy was performed by using a JEM-4000EX (JEOL, Japan) with an acceleration voltage of 400 kV. The nitrogen adsorption and desorption isotherms at the temperature of liquid nitrogen were measured with a Micromeritics ASAP 2010M system. The corresponding pore size distribution curve (30–300 nm) was determined by Hg porosimetry by using a Micromeritics AutoPore IV 9500 system. All samples were out-gassed for 12 h at 150 °C before the measurements. The pore size distribution for mesopores was calculated by using the Barrett-Joyner-Halenda (BJH) model. The pore size distribution for micropores was calculated by using the Horvath-Kawazoe model. Temperature-programmed desorption of ammonia curves were obtained in the range 120–600 °C at a rate of 15 °C min⁻¹.

Acknowledgements

This work was realized in the frame of a Belgian Federal Government (Belspo PAI-IAP) project, INANOMAT, P6/17, and a Belgium-Viet Nam bilateral cooperation project, (BL/13V11). X.-Y.Y. thanks FNRS (Fonds National de la Recherche Scientifique in Belgium) for a "Chargé de Recherche" position. B.L.S. acknowledges the Chinese Central Government for an "Expert of the State" position in the frame of "Thousand Talents Program" and the Chinese Ministry of Education for a "Chang-jiang Chair Visiting Scholar" position at Wuhan University of Technology. We thank Prof. Jing Li and Mrs. Li-Na Wang of the Fourth Military Medical University for their suggestion.

[1] A. Corma, *Chem. Rev.* **1997**, *97*, 2373–2419.

[2] a) M. Hartmann, *Angew. Chem.* **2004**, *116*, 6004–6006; *Angew. Chem. Int. Ed.* **2004**, *43*, 5880–5882; b) C. Madsen, C. J. H. Jacob-

- sen, *Chem. Commun.* **1999**, 673–674; c) B. Su, M. Roussel, K. Vause, X. Yang, F. Gilles, L. Shi, E. Leonova, M. Eden, X. Zou, *Microporous Mesoporous Mater.* **2007**, *105*, 49–57.
- [3] a) X. Yang, Y. Han, K. Lin, G. Tian, Y. Feng, X. Meng, Y. Di, Y. Du, Y. Zhang, F. Xiao, *Chem. Commun.* **2004**, 2612–2613; b) X. Yang, S. Zhang, Z. Qiu, G. Tian, Y. Feng, F. Xiao, *J. Phys. Chem. B* **2004**, *108*, 4696–4700; c) Y. Feng, X. Yang, Y. Di, Y. Du, Y. Zhang, F. Xiao, *J. Phys. Chem. B* **2006**, *110*, 14142–14147.
- [4] S. van Donk, A. Janssen, J. Bitter, K. de Jong, *Catal. Rev.* **2003**, *45*, 297–319.
- [5] C. Jacobsen, C. Madsen, J. Houzvicka, I. Schmidt, A. Carlsson, *J. Am. Chem. Soc.* **2000**, *122*, 7116–7117.
- [6] W. Fan, M. A. Snyder, S. Kumar, P. S. Lee, W. C. Yoo, A. V. McCormick, P. L. Penn, A. Stein, M. Tsapatsis, *Nature Mater.* **2008**, *7*, 984–991.
- [7] S. Kim, H. Shah, T. Pinnavaia, *Chem. Mater.* **2003**, *15*, 1664–1668.
- [8] I. Schmidt, A. Boisen, E. Gustavsson, K. Stahl, S. Pehrson, S. Dahl, A. Carlsson, C. Jacobsen, *Chem. Mater.* **2001**, *13*, 4416–4418.
- [9] A. Sakthivel, A. Huang, W. Chen, Z. Lan, K. Chen, T. Kim, R. Ryoo, A. Chiang, S. Liu, *Chem. Mater.* **2004**, *16*, 3168–3175.
- [10] F. Xiao, L. Wang, C. Yin, K. Lin, Y. Di, J. Li, R. Xu, D. Su, R. Schlögl, T. Yokoi, T. Tatsumi, *Angew. Chem.* **2006**, *118*, 3162–3165; *Angew. Chem. Int. Ed.* **2006**, *45*, 3090–3093.
- [11] M. Choi, H. Cho, R. Srivastava, C. Venkatesan, D. Choi, R. Ryoo, *Nat. Mater.* **2006**, *5*, 718–723.
- [12] B. Holland, L. Abrams, A. Stein, *J. Am. Chem. Soc.* **1999**, *121*, 4308–4309.
- [13] G. S. Zhu, S. L. Qiu, O. Terasaki, *J. Mater. Chem.* **2001**, *11*, 1687–1693.
- [14] a) J. Zhou, Z. L. Hua, X. Z. Cui, Z. Q. Ye, F. M. Cui, J. L. Shi, *Chem. Commun.* **2010**, *46*, 4994–4996; b) A. Sachse, A. Galarneau, *Chem. Mater.* **2010**, *22*, 4123–4125.
- [15] a) X. Yang, A. Leonard, A. Lemaire, G. Tian, B. L. Su, *Chem. Commun.* **2011**, *47*, 2763–2786; b) X. Yang, Y. Li, A. Lemaire, J. Yu, B. L. Su, *Pure Appl. Chem.* **2009**, *81*, 2265–2307.
- [16] J. H. Clark, *Acc. Chem. Res.* **2002**, *35*, 791–797.
- [17] A. Szegedi, M. Hegedus, J. Margitfalvi, I. Kiricsi, *Chem. Commun.* **2005**, 1441–1443.
- [18] R. Mokaya, *Angew. Chem.* **1999**, *111*, 3079–3083; *Angew. Chem. Int. Ed.* **1999**, *38*, 2930–2934.
- [19] R. Ryoo, S. Jun, J. M. Kim, M. J. Kim, *Chem. Commun.* **1997**, 2225–2226.
- [20] W. Li, S. Huang, S. Liu, M. O. Coppens, *Langmuir* **2005**, *21*, 2078–2085.
- [21] a) X. Yang, Y. Li, G. Van Tendeloo, F. Xiao, B.-L. Su, *Adv. Mater.* **2009**, *21*, 1368–1372; b) X. Yang, F. Xiao, B. L. Su, *Catal. Today* **2007**, *128*, 123–128; c) X. Yang, A. Vantomme, A. Lemaire, F. Xiao, B. L. Su, *Adv. Mater.* **2006**, *18*, 2117–2122; d) Y. Li, Q. Yang, J. Yang, C. Li, *Microporous Mesoporous Mater.* **2006**, *91*, 85–91.
- [22] Z. Zhang, Y. Han, L. Zhu, R. Wang, Y. Yu, S. Qiu, D. Zhao, F. Xiao, *Angew. Chem.* **2001**, *113*, 1298–1302; *Angew. Chem. Int. Ed.* **2001**, *40*, 1258–1262.
- [23] Y. Liu, W. Zhang, T. Pinnavaia, *J. Am. Chem. Soc.* **2000**, *122*, 8791–8792.
- [24] T.-O. Do, S. Kaliaguine, *Angew. Chem.* **2001**, *113*, 3348–3351; *Angew. Chem. Int. Ed.* **2001**, *40*, 3248–3251.
- [25] T.-O. Do, S. Kaliaguine, *J. Am. Chem. Soc.* **2003**, *125*, 618–619.
- [26] J. H. Clark, J. C. Ross, D. J. Macquarrie, S. J. Barlow, T. W. Bastock, *Chem. Commun.* **1997**, 1203–1204.
- [27] G. D. Yadav, J. J. Nair, *Microporous Mesoporous Mater.* **1999**, *33*, 1–48.
- [28] J. H. Clark, G. L. Monks, D. J. Nightingale, P. M. Price, J. F. White, *J. Catal.* **2000**, *193*, 348–350.
- [29] S. Pega, C. Boissiere, D. Grosso, T. Azais, A. Chaumonnot, C. Sanchez, *Angew. Chem.* **2009**, *121*, 2822–2825; *Angew. Chem. Int. Ed.* **2009**, *48*, 2784–2787.
- [30] D. C. Sherrington in *Chemistry of Waste Minimisation* (Ed.: J. H. Clark), Blackie Academic, London, **1995**, pp. 141–200.

- [31] a) C. T. Kresge, M. E. Leonowicz, W. J. Roth, J. C. Vartuli, J. S. Beck, *Nature* **1992**, 359, 710–712; b) T. Yanagisawa, T. Shimizu, K. Kuroda, C. Kato, *Bull. Chem. Soc. Jpn.* **1990**, 63, 988–992.
- [32] a) X. Yang, Z. Li, B. Liu, A. Klein-Hofmann, G. Tian, Y. Feng, Y. Ding, D. Su, F. Xiao, *Adv. Mater.* **2006**, 18, 410–414; b) Y. Li, X. Yang, A. Vantomme, J. Yu, G. Van Tendeloo, B. Su, *Chem. Mater.* **2010**, 22, 3251–3258.
- [33] D. Zhao, J. Feng, Q. Huo, N. Melosh, G. H. Fredrickson, B. F. Chmelka, G. D. Stucky, *Science* **1998**, 279, 548–552.
- [34] D. Macquarrie, *Green Chem.* **1999**, 1, 195–198.
- [35] J. Blin, A. Leonard, Z. Y. Yuan, L. Gigot, A. Vantomme, A. Cheetham, B. L. Su, *Angew. Chem.* **2003**, 115, 2978–2981; *Angew. Chem. Int. Ed.* **2003**, 42, 2872–2875; *Angew. Chem. Int. Ed.* **2003**, 42, 2872–2875.
- [36] A. Léonard, B. L. Su, *Chem. Commun.* **2004**, 1674–1675.
- [37] Y. J. Lee, J. S. Lee, Y. S. Park, K. B. Yoon, *Adv. Mater.* **2001**, 13, 1259–1263.
- [38] S. I. Cho, S. D. Choi, J. H. Kim, G. J. Kim, *Adv. Funct. Mater.* **2004**, 14, 49–54.
- [39] A. Dong, Y. Wang, Y. Tang, Y. Zhang, N. Ren, Z. Gao, *Adv. Mater.* **2002**, 14, 1506–1510.
- [40] W. C. Li, A. H. Lu, R. Palkovits, W. Schmidt, B. Spliethoff, F. Schuth, *J. Am. Chem. Soc.* **2005**, 127, 12595–12600.
- [41] Y. C. Tong, T. B. Zhao, F. Y. Li, Y. Wang, *Chem. Mater.* **2006**, 18, 4218–4220.
- [42] Y. Tao, H. Kanoh, K. Kaneko, *J. Am. Chem. Soc.* **2003**, 125, 6044–6045.
- [43] J. Wang, C. Groen, W. Yue, M. O. Coppens, *J. Mater. Chem.* **2008**, 18, 468–474.
- [44] J. Wang, W. Yue, W. Zhou, M. O. Coppens, *Microporous Mesoporous Mater.* **2009**, 120, 19–28.
- [45] A. Dong, Y. Wang, Y. Tang, *Adv. Mater.* **2002**, 14, 926–929.
- [46] N. Kanno, M. Miyake, M. Sato, *Zeolites* **1994**, 14, 625–628.
- [47] A. A. Campos, L. Dimitrov, C. R. Da Silva, M. Wallau, E. A. Urquieta-Gonzalez, *Microporous Mesoporous Mater.* **2006**, 95, 92–103.
- [48] A. A. Campos, L. Martins, L. Lima de Oliveira, C. Ramos de Silva, M. Wallau, E. A. Urquieta-Gonzalez, *Catal. Today* **2005**, 107–108, 759–767.
- [49] T.-O. Do, A. Nossov, M. A. Springuel-Huet, C. Schneider, J. L. Bretherton, C. A. Fyfe, S. Kaliaguine, *J. Am. Chem. Soc.* **2004**, 126, 14324–14325.
- [50] T.-O. Do, S. Kaliaguine, *Angew. Chem.* **2002**, 114, 1078–1082; *Angew. Chem. Int. Ed.* **2002**, 41, 1036–1040.
- [51] L. H. Chen, X. Y. Li, G. Tian, Y. Li, J. C. Rooke, G. S. Zhu, S. L. Qiu, X. Y. Yang, B. L. Su, *Angew. Chem.* **2011**, 123, 11352–11357; *Angew. Chem. Int. Ed.* **2011**, 50, 11156–11161.
- [52] L. H. Chen, X. Y. Li, G. Tian, Y. Li, H. Y. Tan, G. Van Tendeloo, G. S. Zhu, S. L. Qiu, X. Y. Yang, B. L. Su, *ChemSusChem* **2011**, 4, 1452–1456.

Received: May 24, 2011

Revised: August 10, 2011

Published online: November 23, 2011